# Quantitative MRI Establishes the Efficacy of PI3K Inhibitor (GDC-0941) Multi-Treatments in PTEN-deficient Mice Lymphoma

STEPHAN WULLSCHLEGER[1*], JUAN M. GARCÍA-MARTÍNEZ[1*] and SUZANNE L. DUCE[2]

[1]*MRC Protein Phosphorylation Unit, College of Life Sciences, University of Dundee, Dundee, U.K.;*
[2]*Division of Biological Chemistry and Drug Discovery, College of Life Sciences, University of Dundee, Dundee, U.K.*

**Abstract.** *Aim: To assess the efficacy of multiple treatment of phosphatidylinositol-3-kinase (PI3K) inhibitor on autochthonous tumours in phosphatase and tensin homologue (Pten)-deficient genetically engineered mouse cancer models using a longitudinal magnetic resonance imaging (MRI) protocol. Materials and Methods: Using 3D MRI, B-cell follicular lymphoma growth was quantified in a $Pten^{+/-}Lkb1^{+/hypo}$ mouse line, before, during and after repeated treatments with a PI3K inhibitor GDC-0941 (75 mg/kg). Results: Mean pre-treatment linear tumour growth rate was 16.5±12.8 $mm^3$/week. Repeated 28-day GDC-0941 administration, with 21 days 'off-treatment', induced average tumour regression of 41±7%. Upon cessation of the second treatment (which was not permanently cytocidal), tumours re-grew with an average linear growth rate of 40.1±15.5 $mm^3$/week. There was no evidence of chemoresistance. Conclusion: This protocol can accommodate complex dosing schedules, as well as combine different cancer therapies. It reduces biological variability problems and resulted in a 10-fold reduction in mouse numbers compared with terminal assessment methods. It is ideal for preclinical efficacy studies and for phenotyping molecularly characterized mouse models when investigating gene function.*

The genomic era has produced impressive advances regarding our understanding of the genetic factors that contribute to cancer. It has lead to the identification of oncogenes and tumour suppressor genes, and the characterization of the signalling pathways that become ablated or hyperactivated in cancer cells. In turn, this has allowed the development of molecularly targeted anticancer agents that inhibit these aberrant signalling pathways, with the most successful drug being Gleevec® (Novartis, Basel, Swiss). However in the clinic, single molecularly targeted anticancer drug responses have generally been transitory, being followed by relapses (1). Increasingly, the concept of 'one target, one disease' is being challenged (2). There is growing interest in developing new paradigms for anticancer therapies (1-5), for example those that target multiple signalling pathways. Validating and testing the efficacy of these anticancer agents requires molecularly relevant cancer models, which ideally should mimic the genetic mutations that drive cancer growth, as well as replicate the microenvironment of human cancer. In cell cultures, many of the hallmarks of cancer as reviewed by Hanahan and Weinberg (6) cannot be reproduced, such as vasculature and tumour heterogeneity. Moreover, it is becoming apparent that several critical tumorigenesis signalling pathways cannot be observed in 2D cell cultures (7). Consequently, new models, such as molecularly characterized mouse models (8-10) are required for the preclinical testing of the next generation of anticancer therapies.

Subcutaneously xenografted mice with transplanted human cancer cells or tissue are the most common mouse cancer model. Becher and Holland have discussed the limitations of these models (11), which includes the fact that the mice are immunocompromised and so the host's immune system is absent; often the cancer cells are immortalised, and tumours are usually not in their anatomically correct location. The remarkable developments in genetic engineering technology have made it possible to precisely knock-out or overexpress genes in a temporal and spatial manner (12, 13). Thus genetically engineered mice (GEM) are promising alternative cancer models. They are fully immunocompetent and produce integrated orthotopic tumours, although frequently they do not fully replicate human cancer pathology. Two of their main disadvantages are practical. Firstly, it can take many months before spontaneous tumours form. Secondly, unlike tumours in subcutaneous xenograft mouse models where the size of



*These Authors contributed equally to this work.

*Correspondence to:* Dr. Suzanne Duce, Division of Biological Chemistry and Drug Discovery, College of Life Sciences, University of Dundee, Dundee DD1 5EH, U.K. Tel: +44 1382386235, Fax: +44 1382386373, e-mail: s.duce@dundee.ac.uk

*Key Words:* Drug resistance, follicular lymphoma, GDC-0941, mouse cancer model, MRI, PI3K inhibitor, PTEN.

tumours can rapidly be determined using callipers, preclinical imaging such as ultrasound, X-ray computed tomography and magnetic resonance imaging (MRI) are often the only way to non-invasively measure tumour volume in these GEM cancer models (14-17).

The aim of this study was to demonstrate the utility of a 3D MRI protocol for quantitatively phenotyping the growth of autochthonous tumours that form in GEM cancer models, and evaluate its suitability for preclinical studies that involve multiple drug treatment schedules. The mouse model used was a heterozygous *Pten*$^{+/-}$*Lkb1*$^{+/hypo}$ mouse line harbouring a single phosphatase and tensin homologue (*Pten*) allele (18) and 60% reduction in their levels of liver kinase B1 (Lkb1) (19). These mice spontaneously develop large B-cell follicular lymphomas within cervical lymph nodes after about four months. The tumour suppressor gene *PTEN*, which encodes for a lipid phosphatase antagonizing phosphoinositide-3-kinase (PI3K) activity, is one of the most mutated genes in human cancer (20). The PI3K/AKT pathway plays an important role in promoting growth, survival and proliferation of cancer cells, and there is a number of molecularly targeted anticancer agents currently used in clinical trials that inhibit kinases on this pathway (21).

We present data from a three-month longitudinal 3D MRI study to evaluate the efficacy of repeat treatments of PI3K inhibitor GDC-0941 acting on follicular lymphomas that form in the *Pten*$^{+/-}$*Lkb1*$^{+/hypo}$ mouse line, and investigate the potential drug resistance. GDC-0941 selectively inhibits all class 1 PI3K isoforms (22). Preclinical trials have shown that it is well tolerated and slows the growth of several cancer cell lines that have elevated PI3K pathway activity in xenograft mouse models (22, 23). We demonstrated that GDC-0941 produces tumour regression by reducing tumour cell proliferation, promoting apoptosis, and suppressing the centroblast population in B-cell follicular lymphomas (24). GDC-0941 is in clinical evaluations for treatment of non-Hodgkin's lymphomas. According to the American Cancer Society, the overall 5-year relative survival rate for patients with non-Hodgkin' s lymphoma is 63% and the 10-year relative survival rate is 51% (25). GDC-0941 is also used in combination clinical drug trials with other targeted medicines, such as trastuzumab (ClinicalTrials.gov Identifier NCT00928330).

## Materials and Methods

*Mouse breeding and drug treatment*. All animal studies were approved by the University of Dundee Ethics Committee and performed under a UK Home Office project license. The mice were cared for in accordance with Home Office guidelines and standard husbandry practice (26, 27). The generation and genotyping of the *Pten*$^{+/-}$ mice and the *Lkb1* hypomorphic mice have been described previously (18, 28). The parental *Lkb1*$^{+/hypo}$ and *Pten*$^{+/-}$ mice used for these experiments were backcrossed with C57BL/6J mice for over seven generations before initiating the crosses for the present study. These mice express reduced levels of PTEN and LKB1 in all tissues studied (19), and spontaneously develop large B-cell follicular lymphomas within cervical lymph nodes after about four months.

Ten *Pten*$^{+/-}$*Lkb1*$^{+/hypo}$ mice bearing tumours, ranging in age from 7 to 9.5 months and weights from 25 to 30 g, were divided into two groups: the test group (n=6) were given PI3K inhibitor GDC-0941 (GDC-0941 *bis*mesylate at 75 mg/kg), whilst the control group (n=4) were given saline vehicle solution only. The experimental protocol is depicted in Figure 1A, where $\triangle V$ is change in tumour volume and R is tumour growth rate. It includes a pre-treatment phase where tumour growth rates were measured; two treatment stages (treatment 1 and 2) where the efficacy of anticancer agents were determined; and two periods with no treatment (off-treatment 1 and 2) where tumour re-growth was quantified. Day 1 was assigned as the first day the mice were imaged and the mice were imaged three times during the 21-day pre-treatment period, and at intervals between 8 to 15 days thereafter. The mice were treated daily by oral gavage during two 28-day treatment sessions. The first treatment session (treatment 1) ran from day 23 to 50, followed by a 21-day period without any treatment (off-treatment 1). The second 28 day treatment session (treatment 2) was from day 72 to 99, followed by a period without any treatment (off-treatment 2), ending on day 119. At the end of the study, the mice were sacrificed and tumours were extracted and fixed in 10% formalin.

To minimise the problems of biological variability, the cohort groups were all female, with matching genetic profiles. The mice were selected so that each cohort had similar age and tumour size profiles. The handling procedures for all the mice were the same. The treatment cohort size was similar to the recommendations made by the International Mouse Phenotyping Consortium (IMPC), based on the European Mouse Disease Clinic investigations into statistical impact and reliability of cohort size (29). During the course of the study, the 10 mice generated 104 data points, which with single data-point post-mortem methods would have involved 104 mice.

*MRI and data analysis*. Mice were anaesthetized with 1.5% isoflurane in 100% oxygen using a nose cone; scavenging was used to remove the anaesthetic after use. The mice were appropriately restrained in a mouse cradle using a bite bar and tape to minimise motion. Mouse physiology was monitored during imaging and recovery periods, and mice were returned to their cages when fully recovered. The MRI data were acquired on a Bruker Avance FT NMR spectrometer (Bruker Biospin GmbH, Rheinstetten, Germany) with a wide-bore 7.1 T vertical-axis magnet resonating at 300.15 MHz for $^{1}$H. A Bruker MicroMouse birdcage radio-frequency resonator with an internal diameter of 30 mm was used. 3D 128 by 128 by 128 rapid acquisition relaxation enhanced (RARE) MRI experiments were performed with RARE factor of 4. Repetition time (TR) of 250 ms and an effective echo time (TE) of 10 ms were used. One acquisition sequence was acquired to minimise the experimental time, which was 16 min. The field of view was 30 mm and the isotropic image spatial resolution was 234 μm per pixel.

The Fourier-transformed MRI data were visualised using the Amira PC-based software (Visage Imaging GmbH, 12163 Berlin, Germany). This permitted 2D slices to be viewed from any orientation within the 3D data set, and the anatomy of interest to be digitally segmented. The ID numbers of the mice and the time points were known, but their treatment histories were unknown to the person who performed the data processing, so data analysis was not completely blind. 3D surface representations of anatomical structures were produced by surface rendering the 3D finite element meshes generated from the segmentation of the regions of interest. This allowed volumes to be determined. The segmentation was semi-automated starting with signal

Table I. *Cervical lymphoma volumes ($mm^3$) of control and test cohorts at each time point. Control cohort A-D (n=4) was treated with saline vehicle alone and the test cohort A-F (n=6).*

| Day | Control mice | | | | Test mice | | | | | |
|---|---|---|---|---|---|---|---|---|---|---|
| | A | B | C | D | A | B | C | D | E | F |
| 1 | 163.9 | 283.1 | 78.8 | 158.9 | 233.8 | 136.1 | 273.4 | 150.9 | 151.4 | 176.8 |
| 14 | 172 | 317.9 | 109.3 | 180.4 | 245.8 | 173.8 | 339.4 | 163.8 | 158.8 | 193.3 |
| 23 | 182.4 | 341.3 | 113.3 | 200.8 | 259.4 | 190.4 | 409.3 | 191.4 | 180.8 | 203.8 |
| 37 | 190.2 | 391.5 | 125.7 | 191.2 | 145.3 | 126.6 | 218.8 | 100.4 | 108.4 | 110.3 |
| 51 | 202.4 | 441.7 | 158.7 | 221.7 | 139.7 | 123.2 | 188.4 | 86.2 | 106.8 | 91 |
| 63 | 206.3 | | 165.5 | 236.5 | 247.2 | 170.9 | 256.2 | 155.4 | 144.3 | 126.6 |
| 72 | 217.8 | | 180.9 | 248.1 | 263.6 | 214.3 | 294.2 | 190.6 | 170.7 | 140 |
| 87 | 236.5 | | 187.2 | 252.8 | 170.7 | 150.9 | 189.4 | 109.6 | 102.5 | 93.9 |
| 100 | 250.5 | | 191.7 | 255.3 | 154.9 | 151 | 174.3 | 94.4 | 92.8 | 88.2 |
| 111 | 257.5 | | 217 | 261.2 | 256.3 | 195.5 | 246.5 | 162 | 141.4 | 110.8 |
| 119 | 258.4 | | 232 | 263.5 | 298.1 | 252.5 | 327.3 | 202.9 | 169 | 130.2 |

Table II. *Murine cervical follicular lymphoma growth rates ($mm^3$/week) during pre-treatment, and off-treatment periods 1 and 2. The test cohort mice A-F received GDC-0941 (75 mg/kg).*

| Tumour growth rate ($mm^3$/week) | Test mice | | | | | |
|---|---|---|---|---|---|---|
| | A | B | C | D | E | F |
| Pre-treatment (R1) | 8 | 17.5 | 41.3 | 12.5 | 9 | 8.6 |
| Off-treatment 1 (R2) | 44.3 | 31.8 | 37.3 | 36.8 | 22.4 | 17.4 |
| Off-treatment 2 (R3) | 56.3 | 39.1 | 56.4 | 42.4 | 29.8 | 16.3 |

intensity thresholding methods proceeded by a manual 'painting' method. Partial volume effects, chemical shift artefacts, radio frequency coil inhomogeneities and mouse movement were identified as the main sources of errors. Previous reproducibility studies of *in vivo* kidney volumes measured by same MRI protocol using 'test-retest' triplicate experiments with this preclinical scanner had an estimated fractional 95% confidence interval of the order of 14% (30). Mean tumour volumes and growth rates were calculated; standard deviations (sd) are quoted. The two-tailed, unpaired *t*-test was used to statistically compare the differences between two different groups using GraphPad software (La Jolla, California, USA). A *p*-value of less than 0.05 was considered significant.

## Results and Discussion

The B-cell follicular lymphomas in the neck region of heterozygous $Pten^{+/-}Lkb1^{+/hypo}$ mice were visualised over a 17-week period at intervals of between 8 and 15 days. The echo and recycle times had been optimised to maximise contrast between tissue types and ensure the boundary of the tumour could be identified (Figure 2A). The tumours have a darker appearance than the neighbouring sub-maxillary and sub-lingual salivary glands, the average contrast resolution (to noise) was 8:1. The average signal-to-noise ratio of B-cell follicular lymphomas in T2-weighted MRI was 16:1. The subcutaneous adipose tissue is white and clearly distinguishable from the lymphomas as the contrast resolution (to noise) was of the order of 42:1. The high image intensity of lipids in the adipose tissue produces chemical shift artefacts along the read magnetic field gradient axis (sagittal), and also introduces partial volume problems. The mice were sacrificed at the end of the study to extract the tumours; the *ex vivo* image (Figure 2B) can be compared with that of day 119 (Figure 2A).

Amira software was used to digitally segment the tumours ventral to the salivary glands. Representative images from control and test mice at day 1, 23 and 51 are displayed in Figure 1C, with tumours shown in pink. The tumour volumes were calculated for each mouse at each time point and tabulated (Table I). Relative tumour volumes were calculated by assigning the tumour volume at the start of treatment 1, on day 23, as 1. The changes in the mean relative tumour volumes of the control and test groups with time are shown in Figure 1B. The tumour growth for the control cohort was linear with a mean growth rate of 13.9±10.9 $mm^3$/week, (coefficient of determination $R^2$=0.9864; the *t*-test showed the linear correlation was highly statistically significant). Unsurprisingly the saline treatment had no effect on tumour growth. By the end of the study, tumours in saline-treated mice had on average nearly doubled (1.9) in size. Each mouse was individually phenotyped; the tumour growth rates of the six test mice before the start of the GDC-0941 treatment are shown in Table II. Despite these mice being genetically similar, their tumour growth rates range between 8

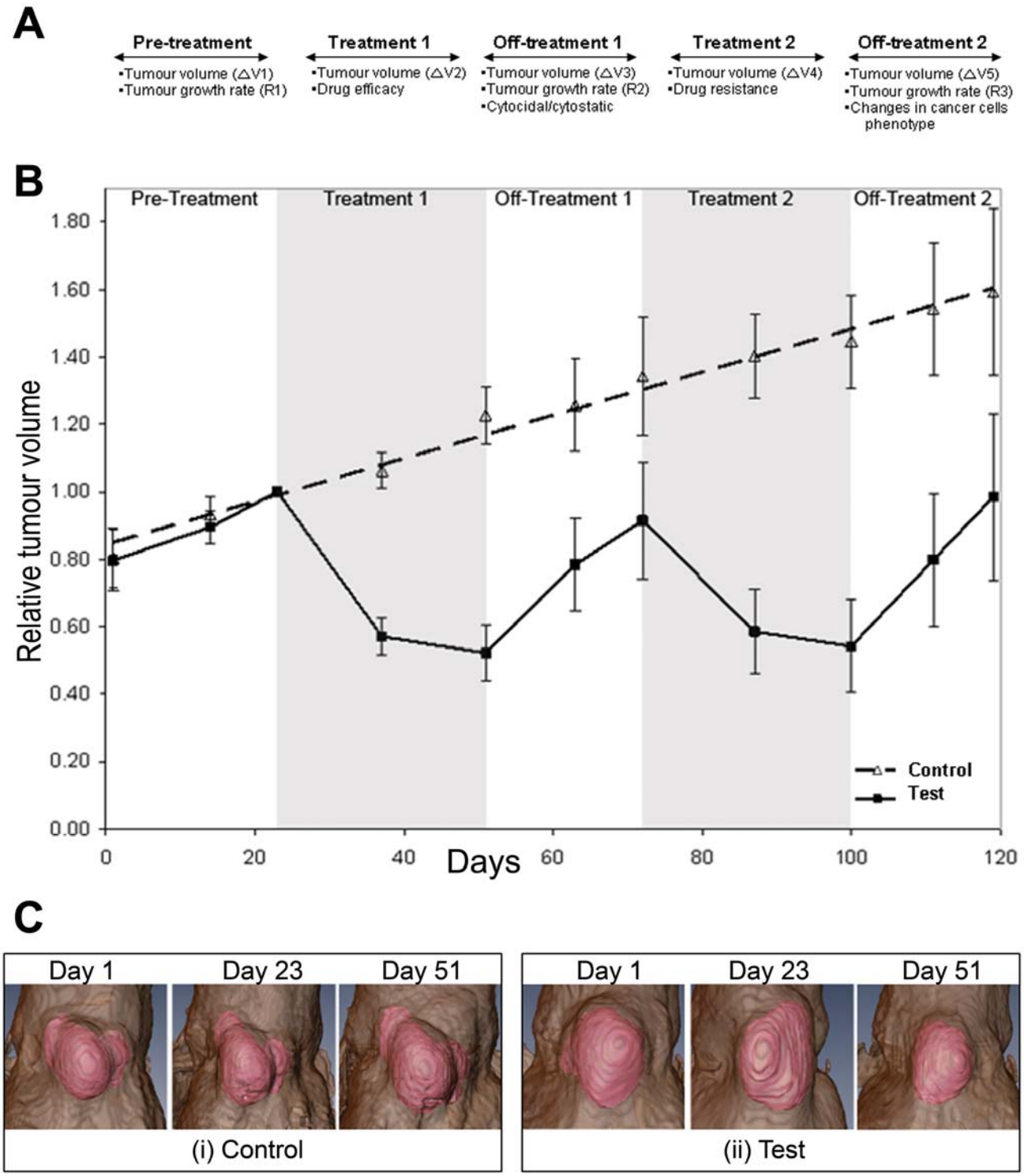


Figure 1. *Longitudinal study of tumour regression induced by oral administration of GDC-0941. A: Longitudinal protocol (△V is change in tumour volume, R is tumour growth rate). B: Mean relative tumour volumes (normalised to size at day 23, at the start of treatment 1) plotted against time. Control cohort was treated with vehicle alone (n=4). Test cohort was treated with GDC-0941 at 75 mg/kg (n=6). Errors bars are standard deviations. C: Ventral transverse views of 3D surface reconstructions of RARE-4 MRI data set of the neck region of heterozygous $Pten^{+/-}Lkb1^{+/hypo}$ mice bearing tumours: (i) control mouse and (ii) test mouse. The skin is shown in brown and tumours in pink. Control cohort received saline vehicle and the test cohort received GDC-0941 (75 mg/kg). The start of: pre-treatment was day 1, treatment 1 was day 23, off-treatment 1 was day 51, treatment 2 was day 72, off-treatment 2 was day 100, and the end of off-treatment 2 was day 119.*


Figure 2. *Ventral transverse views of neck of heterozygous Pten$^{+/-}$Lkb1$^{+/hypo}$ mouse. A: 2D MRI images from RARE-4 MRI data set acquired on day 119. B: Image of tumours during extraction. t, tumours; sg, sub-maxillary salivary gland; j, jaw; a, subcutaneous adipose tissue.*

and 41 mm$^3$/week, with an average linear growth rate of 16.5±12.8 mm$^3$/week (R1) (*R2*=0.987).

During treatment 1, the tumours in the GDC-0941-treated mice showed a marked non-linear shrinkage, with an average tumour regression of 52±8%. This tumour regression profile had been observed previously, with shrinkage reaching a plateaus after a month (24). When the GDC-0941 treatment ceased, the tumours in the test cohort mice grew again (off-treatment period 1) with an average linear tumour growth rate of 31.3±9.9 mm$^3$/week (R2) (*R2*=0.98). R2 for individual GDC-0941 test mice are shown in Table II. After 21 days, the tumours had nearly returned to their size at the start of treatment. They grew on average nearly twice (1.9) as fast as before treatment (R2>R1); the difference was statistically significant ($p$=0.042). As with many molecular-targeted anticancer therapies, GDC-0941 stopped cells' proliferation but was not completely cytocidal.

The test mice started their second GDC-0941 chemotherapy course on day 72 (treatment 2) and tumours regressed with average tumour shrinkage of 41±7% (Figure 2B). Treatment 2 produced slightly better tumour regression than treatment 1, with similar regression profiles; so it would appear that that the tumours had not become resistant to the PI3K inhibitor and that the drug action was similar during both treatments. At the end of the second treatment (off-treatment 2), the lymphomas in the GDC-0941-treated mice grew with an average linear growth rate of 40.1±15.5 mm$^3$/week (R3) (*R2*=0.958). This was on average 28% faster than the tumour growth after the first drug treatment (R3>R2). The difference between R1 and R2 growth rates was statistically significant ($p$=0.0157) but difference between R2 and R3 was not. R3 for individual GDC-0941 test mice are also shown in Table II. The difference in tumour growth rates R1 and R3 could be due to the fact that the phenotype of the tumour cells had changed as a result of drug treatment, and the remaining tumour cells were more aggressive. Alternatively, the tumour microenvironment may have changed, which made it more conducive for tumour growth. Since no resistance to the PI3K inhibitor was observed and tumour re-growth rates as a result of treatments 1 and 2 were quite similar, it suggested that a change in the tumour microenvironment is more likely to be responsible for the increase in growth rate.

## Conclusion

In summary, this study demonstrates the utility of *Pten*-deficient mouse lines as a preclinical cancer model of B-cell follicular lymphomas. The longitudinal MRI drug protocol described in Figure 1A is an effective method for quantitatively evaluating multiple treatments with GDC-0941, and allowed potential mode of action and chemoresistance to be investigated. The GDC-0941 treatments produced tumour regression of approximately 50%, but the PI3K inhibitor did not produce permanent tumour shrinkage. Although the tumour growth rate increased after each drug treatment (R1<R2<R3), repeating treatment did not induce chemo-resistance and the differences might be due to changes in the tumour microenvironment.

The strength of this technique is the non-invasive nature of MRI, so that the same animals can be used throughout. This resulted in a 10-fold reduction in mouse numbers required for the study compared with terminal assessment methods; this is in line with the 3Rs principle (Replacement, Reduction and Refinement). The mice themselves act as internal controls which reduces problems of biological variability, especially useful when considering the variation in growth rates between different tumours. This protocol is able to accommodate complex drug dosing schedules and multiple drug combinations, as well as different cancer therapies. This longitudinal method can often detect subtle changes that may be lost when combining data from single data-point methods. In conclusion, we suggest that this MRI protocol is well suited for preclinical efficacy studies of the next generation of anticancer therapies. It can also be applied to gene function

studies when used to phenotype different GEM models (31) during investigation of genotype-to-phenotype relationships.

## Conflict of Interest

The Authors declare that they have no competing or financial interests relating to the work in this publication.

## Acknowledgements

We would like to thank Dario Alessi and Stewart Fleming for helpful discussions. We acknowledge the help of Natalia Shpiro for synthesis of GDC-0941 bismesylate and Marek Gierlinski (Data Analysis Group). We also thank the Medical Research Council (SW, JMGM), Wellcome Trust (SLD) and the pharmaceutical companies supporting the Division of the Signal Transduction Therapy Unit (AstraZeneca, Boehringer-Ingelheim, GlaxoSmithKline, Merck-Serono and Pfizer) for financial support.

## References

1 Kummar S, Chen HX, Wright J, Holbeck S, Millin MD, Tomaszewski J, Zweibel J, Collins J and Doroshow JH: Utilizing targeted cancer therapeutic agents in combination: novel approaches and urgent requirements. Nat Rev Drug Discov *9*: 843-856, 2010.

2 Hopkins AL: Network pharmacology: the next paradigm in drug discovery. Nat Chem Biol *4*: 682-690, 2008.

3 Levitzki A and Klein S: Signal transduction therapy of cancer. Mol Aspects Med *31*: 287-329, 2010.

4 de Bono JS and Ashworth A: Translating cancer research into targeted therapeutics. Nature *467*: 543-549, 2010.

5 Prendergast G: Cancer Therapeutics: Strategies for Drug Discovery and Development. New Jersey: Wiley-Blackwell, 2004.

6 Hanahan D and Weinberg RA: Hallmarks of cancer: The next generation. Cell *144*: 646-674, 2011.

7 Gilbert CA, Daou M-C, Moser RP and Ross AH: γ-secretase inhibitors enhance temozolomide treatment of human gliomas by inhibiting neurosphere repopulation and xenograft recurrence. Cancer Res *70*: 6870-6879, 2010.

8 Cheon D-J and Orsulic S: Mouse models of cancer. Annu Rev Pathol *6*: 95-119, 2011.

9 Frese KK and Tuveson DA: Maximizing mouse cancer models. Nat Rev Cancer *7*: 645-658, 2007.

10 Sharpless NE and DePinho RA: Model organisms - The mighty mouse: genetically engineered mouse models in cancer drug development. Nat Rev Drug Discov *5*: 741-754, 2006.

11 Becher OJ and Holland EC: Genetically engineered models have advantages over xenografts for preclinical studies. Cancer Res *66*: 5526-5526, 2006.

12 Sundberg J and Tsutomu I: Genetically Engineered Mice Handbook. Florida: CRC Press, 2005.

13 Skarnes WC, Rosen B, West AP, Koutsourakis M, Bushell W, Iyer V, Mujica AO, Thomas M, Harrow J, Cox T, Jackson D, Severin J, Biggs P, Fu J, Nefedov M, de Jong PJ, Stewart AF and Bradley A: A conditional knockout resource for the genome-wide study of mouse gene function. Nature *474*: 337-361, 2011.

14 Koo V, Hamilton PW and Williamson K: Non-invasive *in vivo* imaging in small animal research. Cell Oncol *28*: 127-139, 2006.

15 Henkelman RM: Systems biology through mouse imaging centers: Experience and new directions. Annu Rev Biomed Eng *12*: 143-166, 2010.

16 Marcus CD, Ladam-Marcus V, Cucu C, Bouche O, Lucas L and Hoeffel C: Imaging techniques to evaluate the response to treatment in oncology: Current standards and perspectives. Crit Rev Oncol Hematol 72: 217-238, 2009.

17 Lyons SK: Advances in imaging mouse tumour models *in vivo*. J Pathol 205: 194-205, 2005.

18 Podsypanina K, Ellenson LH, Nemes A, Gu JG, Tamura M, Yamada KM, Cordon-Cardo C, Catoretti G, Fisher PE and Parsons R: Mutation of Pten/Mmac1 in mice causes neoplasia in multiple organ systems. Proc Natl Acad Sci USA *96*: 1563-1568, 1999.

19 Huang X, Wullschleger S, Shpiro N, McGuire VA, Sakamoto K, Woods YL, McBurnie W, Fleming S and Alessi DR: Important role of the LKB1-AMPK pathway in suppressing tumorigenesis in PTEN-deficient mice. Biochem J *412*: 211-221, 2008.

20 Keniry M and Parsons R: The role of PTEN signaling perturbations in cancer and in targeted therapy. Oncogene *27*: 5477-5485, 2008.

21 Matthews DJ and Gerritsen ME: Targeting Protein Kinases for Cancer Therapy. New Jersey: Wiley-Blackwell, 2010.

22 Folkes AJ, Ahmadi K, Alderton WK, Alix S, Baker SJ, Box G, Chuckowree IS, Clarke PA, Depledge P, Eccles SA, Friedman LS, Hayes A, Hancox TC, Kugendradas A, Lensun L, Moore P, Olivero AG, Pang J, Patel S, Pergl-Wilson GH, Raynaud FI, Robson A, Saghir N, Salphati L, Sohal S, Ultsch MH, Valenti M, Wallweber HJA, Wan NC, Wiesmann C, Workman P, Zhyvoloup A, Zvelebil MJ and Shuttleworth SJ: The identification of 2-(1H-indazol-4-yl)-6-(4-methanesulfonyl-piperazin-1-ylmethyl)-4-morpholin-4-yl-thieno[3,2-d]pyrimidine (GDC-0941) as a potent, selective, orally bioavailable inhibitor of class I PI3 kinase for the treatment of cancer. J Med Chem *51*: 5522-5532, 2008.

23 Salphati L, Wong H, Belvin M, Bradford D, Edgar KA, Prior WW, Sampath D and Wallin JJ: Pharmacokinetic-pharmacodynamic modeling of tumor growth inhibition and biomarker modulation by the novel phosphatidylinositol 3-kinase inhibitor gdc-0941. Drug Metab Dispos *38*: 1436-1442, 2010.

24 Garcia-Martinez JM, Wullschleger S, Preston G, Guichard S, Fleming S, Alessi DR and Duce SL: Effect of PI3K-and mTOR-specific inhibitors on spontaneous B-cell follicular lymphomas in PTEN/LKBI-deficient mice. Br J Cancer *104*: 1116-1125, 2011.

25 American Cancer Society: Non-Hodgkin Lymphoma. Atlanta: American Cancer Society, 2011.

26 Kilkenny C, Browne WJ, Cuthill IC, Emerson M and Altman DG: Improving bioscience research reporting: the ARRIVE guidelines for reporting animal research. PLoS Biol *8*: 1000412, 2010.

27 Workman P, Aboagye EO, Balkwill F, Balmain A, Bruder G, Chaplin DJ, Double JA, Everitt J, Farningham DAH, Glennie MJ, Kelland LR, Robinson V, Stratford IJ, Tozer GM, Watson S, Wedge SR and Eccles SA: Guidelines for the welfare and use of animals in cancer research. Br J Cancer *102*: 1555-1577, 2010.

28 Sakamoto K, McCarthy A, Smith D, Green KA, Hardie DG, Ashworth A and Alessi DR: Deficiency of LKB1 in skeletal muscle prevents AMPK activation and glucose uptake during contraction. EMBO J *24*: 1810-1820, 2005.

29 Moore M and and IMPC Steering Committee: The International Mouse Phenotyping Consortium Initial Business Plan. Harwell, 2010.

30 He L: Quantitative Investigation of the Accuracy and Precision of Volumetric Studies Using Magnetic Resonance Imaging. MSc Thesis, University of Dundee, UK, 2011.

31 Wullschleger S, Sakamoto K, Johnstone L, Duce S, Fleming S and Alessi DR: How moderate changes in Akt T-loop phosphorylation impact on tumorigenesis and insulin resistance. Dis Model Mech *4*: 95-103, 2011.

*Received November 26, 2011*
*Revised December 19, 2011*
*Accepted December 21, 2011*